JOURNAL OF GEOPHYSICAL RESEARCH, VOL. 102, NO. D12, PAGES 13,581–13,593, JUNE 27, 1997

A study of composite cirrus morphology using data from a 94-GHz radar and correlations with temperature and large-scale vertical motion

Gerald G. Mace,[1] Thomas P. Ackerman, and Eugene E. Clothiaux
Department of Meteorology and Earth System Science Center, The Pennsylvania State University, University Park

Bruce A. Albrecht
University of Miami

Abstract. In order to improve the representation of clouds in climate models, we require a better understanding of the relationship among cloud properties and the synoptic-scale state of the atmosphere. In order to investigate this issue as it pertains to a specific class of cirrus clouds, we have combined a 2 month data set of radar reflectivities observed at State College, Pennsylvania, using a W-band radar with output from a mesoscale model that uses 3-hourly data assimilation. Products of the analysis include statistical distributions of fundamental cirrus cloud properties, such as frequency of occurrence, base, top and midcloud height, and layer thickness. We also consider the relationships between cirrus reflectivity and the large-scale meteorological state defined by area-averaged temperature and vertical velocity. Overall, cirrus clouds are observed 32% of the time, and 51% of those events occur in conjunction with lower-level clouds. Most of the cirrus occur in thin layers (<1.5 km thickness). Cirrus occurrence appears to be related to large-scale meteorological factors but the relationships are complex. The majority of the cirrus we observed occurred at temperatures lower than -35°C and there is little correlation between radar reflectivity and temperature. We also used this data set to examine the usefulness of a satellite-borne W-band radar.

Introduction

Clouds can be described on multiple spatial and temporal scales. The patterns of cloud systems seen on satellite imagery are related to the synoptic scale motions of the atmosphere. While these familiar patterns are modulated by mesoscale atmospheric features, individual cloud elements are maintained through a coupling between turbulent motions, water vapor availability, and aerosol characteristics on much smaller scales. The study of clouds has tended to concentrate at either end of this scale continuum. Since the advent of satellites, many investigators have documented the statistical occurrence of clouds over the planet [e.g., *Wylie and Menzel*, 1989] and their influence on the earth radiation budget [e.g., *Ramanathan et al.*, 1989]. Because the vertical extent and structure of clouds cannot be addressed easily from satellite radiances, this aspect of cloud properties has been addressed in recent years by several field programs using instrumented aircraft and supporting ground-based remote sensors [*Randall et al.*, 1995].

While the results of past studies have significantly advanced our understanding of the role of clouds in the climate system, many questions remain unanswered. For instance, the coupling of microphysical and macroscopic cloud characteristics to the meso-synoptic atmospheric state is still largely undetermined from data. There exists little published literature which simultaneously documents the occurrence of multiple cloud layers, cloud base heights, cloud top heights, and internal cloud structures, within a rigorously defined meteorological context. While this is not surprising given the limitations of conventional observational methodologies, it is precisely this coupling between large-scale atmospheric characteristics and the structure of cloud systems that must be understood before the role of clouds in the climate system can be fully described and their representation in climate models improved.

Recent advances in the development of short wavelength radars allows us to address one aspect of this issue. In this paper we use an extensive set of observations from a surface-based 94-GHz radar to examine the composite vertical structure of cirrus clouds and attempt to place this composite description within an appropriate meteorological setting. Specifically, we consider the frequency distributions of the cloud geometric properties, the relationship between cirrus occurrence and the large-scale vertical motion, and the distribution of radar reflectivity as a function of temperature. We interpret these distributions relative to a simple conceptual model of cirrus clouds and critically evaluate the assumptions underlying a number of cirrus parameterizations designed for large-scale atmospheric models. Additionally, we consider the utility of a satellite-borne 94-GHz radar.

Data and Analysis Techniques

Short wavelength radars designed for the remote sensing of cloud properties bypass many of the difficulties of more conventional observational techniques [*Kropfli*, 1995]. These remote sensing systems, operating typically in the Ka- and W-bands, are

[1]Now at Department of Meteorology, University of Utah, Salt Lake City.

Paper number 97JD00402.
0148-0227/97/97JD-00402$09.00

able to sense multiple, optically-thick cloud layers and collect data continuously. For this study, we used data from the Pennsylvania State University 94-GHz (3-mm wavelength) Doppler radar [*Clothiaux et al.*, 1995]. We operated the radar nearly continuously from a site in central Pennsylvania in a vertically pointing mode from early October through mid-December, 1994, with a primary goal of characterizing continental stratocumulus clouds. During this period, we also collected an extensive record of cirrus cloud reflectivities.

The fundamental atmospheric quantity that we can infer from radar power measurements is the back-scattering cross section per unit volume or radar reflectivity, η. We choose to express our measurements of η in terms of the equivalent radar reflectivity factor, Z_e, which is defined by

$$Z_e = (\lambda^4 / \pi^5)|K_w|^2 \eta .$$

Here λ is the radar wavelength, and K_W is related to the refractive index of water [*Doviak and Zrnic*, 1993]. For spherical particles that are small compared to the radar wavelength, Z_e is identical to the radar reflectivity factor Z, expressed as

$$Z = \int_{D\,\mathrm{min}}^{D\,\mathrm{max}} N(D) D^6 dD,$$

where $N(D)dD$ is the number of particles per unit volume within the size range dD. *Atlas et al.* [1995] show that the scattering of 94-GHz radar energy by typical cirrus crystal populations can be approximated reasonably well by the assumption that the particles are small with respect to the wavelength; hence Z_e in this data set is generally proportional to the sixth moment of the size distribution. Since ice water content (IWC) is proportional to the third moment of the size distribution, Z_e and IWC are correlated, although the exact numerical relationship between the two for any given cirrus cloud, or the data set in general, cannot be specified accurately from radar reflectivity alone [*Atlas et al.*, 1995].

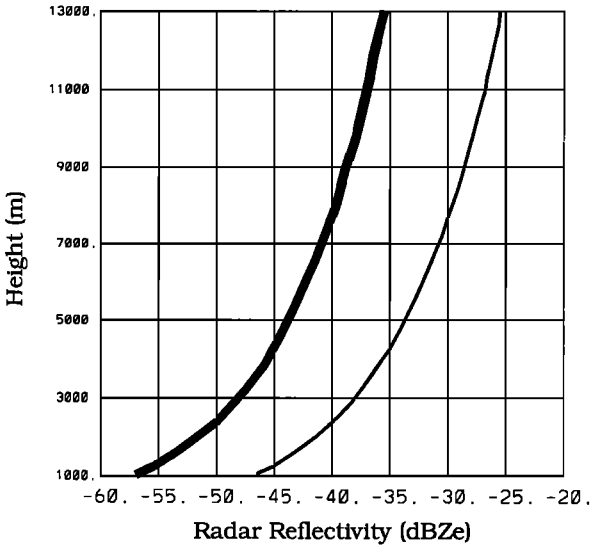

Figure 1. The minimum detectable signal of the Pennsylvania State University W-band radar accounting for loss due to the bistatic offset. The thin solid line shows the minimum detectable signal using 2000 pulse averages and a 0.5-μs pulse width and the heavy solid line shows the minimum detectable signal using 50,000 pulse averages and a 0.95-μs pulse width.

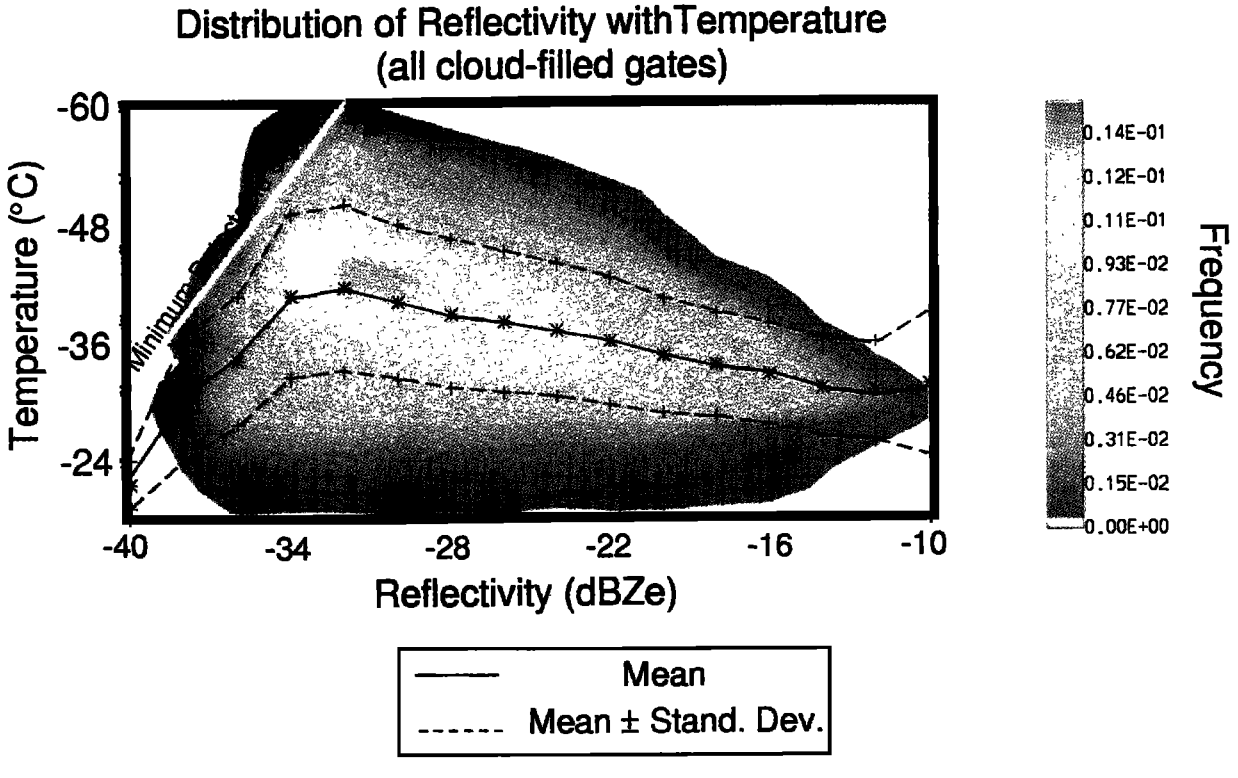

Plate 1. Reflectivity-Temperature frequency histogram for all cirrus observations collected during the autumn 1994 observing period. The solid line denotes the mean reflectivity as a function of temperature and the dashed lines denote plus and minus 1 standard deviation from the mean.

The radar reflectivity profiles collected during the study period consist of averages of approximately 2000 pulses. Depending on the pulse repetition frequency of the radar, these pulses are evenly distributed over an 8 to 12 second interval. During the study period, the radar was operated with pulse lengths of 0.5 and 1 μs and the range gate spacing varied between 30 and 75 meters. The minimum detectable signal of a radar can be expressed [*Clothiaux et al.*, 1995],

$$\overline{P_{min}(mW)} = \frac{1.28\overline{P_n}}{N^{1/2}}$$

where P_n is the system noise power and N is the number of pulses per range gate sample. Using a typical noise power of 4.7×10^{-10} mW calculated from cloud-free range gates, the thin solid curve in Figure 1 shows the minimum detectable signal of the radar for 2000 pulse averages and a 0.5μs pulse. At cirrus levels, the minimum detectable signal is well within the range of reflectivities expected for thin cirrus [*Atlas et al.*, 1995] and a significant fraction of the cirrus will be missed. To increase our sensitivity to thin cirrus, we consider 50,000 pulse averages constructed by calculating the mean analog to digital converter counts for the appropriate number of archived profiles. Increasing the number of averaged pulses in each profile significantly reduces the minimum detectable signal as shown in Figure 1, although the temporal averaging increases to approximately 5 min. The longer averaging period, however, ensures that each profile is more representative of the cirrus layer as a whole instead of a short snapshot that contains detail on only the most reflective regions of the layer. A long time
series of these averaged profiles are then used as input to the cloud mask algorithm described by *Clothiaux et al.* [1995]. Using an estimate of the instrument noise calculated as the mean of the contiguous 25 gates near the top of the profile with the lowest signal, the radar reflectivity is calculated for all gates deemed to contain significant return by the cloud mask algorithm.

Clothiaux et al. [1995] report that the absolute calibration of the Pennsylvania State University radar is known to within 4 dB when extinction of the radar beam by atmospheric gasses and hydrometeors is known. Comparison of Pennsylvania State University radar reflectivity observations with observations by the University of Massachusetts W-band radar [*Sekelsy and McIntosh*, 1996] during April 1995 suggests that the PSU reflectivity estimates are biased low by approximately 4 dB. This bias is also evident in comparisons of PSU radar reflectivity observations with reflectivities derived from in situ observations collected by the University of Wyoming King Air Turbo Prop during April 1995. Therefore we add a 4-dB correction to all radar reflectivity observations considered in this study. Two-way losses due to water vapor and oxygen absorption are calculated using the technique of *Schroeder and Westwater* [1991] with thermodynamic soundings estimated using the Rapid Update Cycle model output (use of this model is discussed in more detail below). The distribution of liquid water is not known; hence we make no attempt to correct the reflectivity profiles for attenuation by liquid water. However, the radar was operated next to a 9-channel microwave radiometer from which we can deduce the total path value of condensed liquid above the radar. With this information, we screen the data for periods when cloud water caused substantial attenuation. Therefore we delete any reflectivity profile from the time series if either the precipitable liquid water exceeds 0.5 mm (corresponding roughly to a 3-dB Z_e two way loss) or the total reflectivity below cirrus levels exceeds -20 dB *Ze*. This constraint accounts for thick ice and mixed phase clouds below cirru levels that are not observed by the microwave radiometer. Consequently, the reflectivity observations reported here are at most biased low by 3 dB Z_e, with most observations having much less bias.

To place the radar time series within a larger-scale meteorological context, we operationally collected Rapid Update Cycle (RUC) model output [*Benjamin et al.*, 1990] from the National Meteorological Center. The RUC model is a data assimilation mesoscale model with a horizontal resolution of 60 km and 25 vertical levels that are defined using mixed sigma and isentropic coordinates. The assimilated data comes from both synoptic data (radiosondes and surface observations) and asynoptic observations, such as surface aviation hourlies, wind profiler data, and aircraft reports. The RUC model is reinitialized every 3 hours, and its output is made available by anonymous ftp in hourly files. The model output used here consists of the initial model field plus the consecutive 1- and 2-hour forecasts. Gridpoint profiles in a 200-km region surrounding the radar site at State College, Pennsylvania, are extracted from the model output and interpolated to geometric height coordinates. Using a linear least squares regression scheme described by *Thiebaux and Pedder* [1987], we calculate the spatially averaged profiles of wind, temperature, and pressure, as well as their gradients, that are valid on synoptic scales. The vertical motion is calculated from the spatially averaged divergence profile using a kinematic technique [*Mace et al.*, 1995], and the tropopause height is determined by identifying the most significant discontinuity in the potential vorticity profile above 9 km [*Hoskins et al.*, 1985]. We chose the scale of dynamical analysis to be 200 km both to mimic the current resolution of typical general circulation models (GCMs) and to reduce the uncertainty in the horizontal divergence and the resulting large-scale vertical velocity by using spatially averaged model profiles.

Our goal is to examine the composite structure of upper tropospheric clouds that are isolated vertically in their reflectivity profile from other lower-level clouds. Deep cloud systems such as altostratus or nimbostratus, while certainly cirrus-topped much of the time, are not the focus of this study. Other investigators have used a combination of visual inspection and height

Table 1. Cirrus Occurrence Frequencies, Means, and Standard Deviations

	Mean	Standard Deviation
Fraction of observations, %	32	
Cirrus with lower clouds, %	52	
Multiple cirrus Layers, %	21	
Cirrus base, km	8.5	1.1
Cirrus top, km	9.9	1.1
Cloud top-tropopause distance, km	1.6	1.1
Midcloud height, km	9.2	1.1
Layer thickness, km	1.6	1.3
Temperature, °C	-40	7.3
Reflectivity, dB Z_e	-26.3	-24.1
Large-scale vertical velocity, cm/s	+ 0.7	4.1

Cirrus Statistics compiled from the 899 hour autumn 1994 cloud radar data set (see the text for a complete explanation). The cirrus with lower clouds and the multiple cirrus layers are given as a fraction of the observed cirrus.

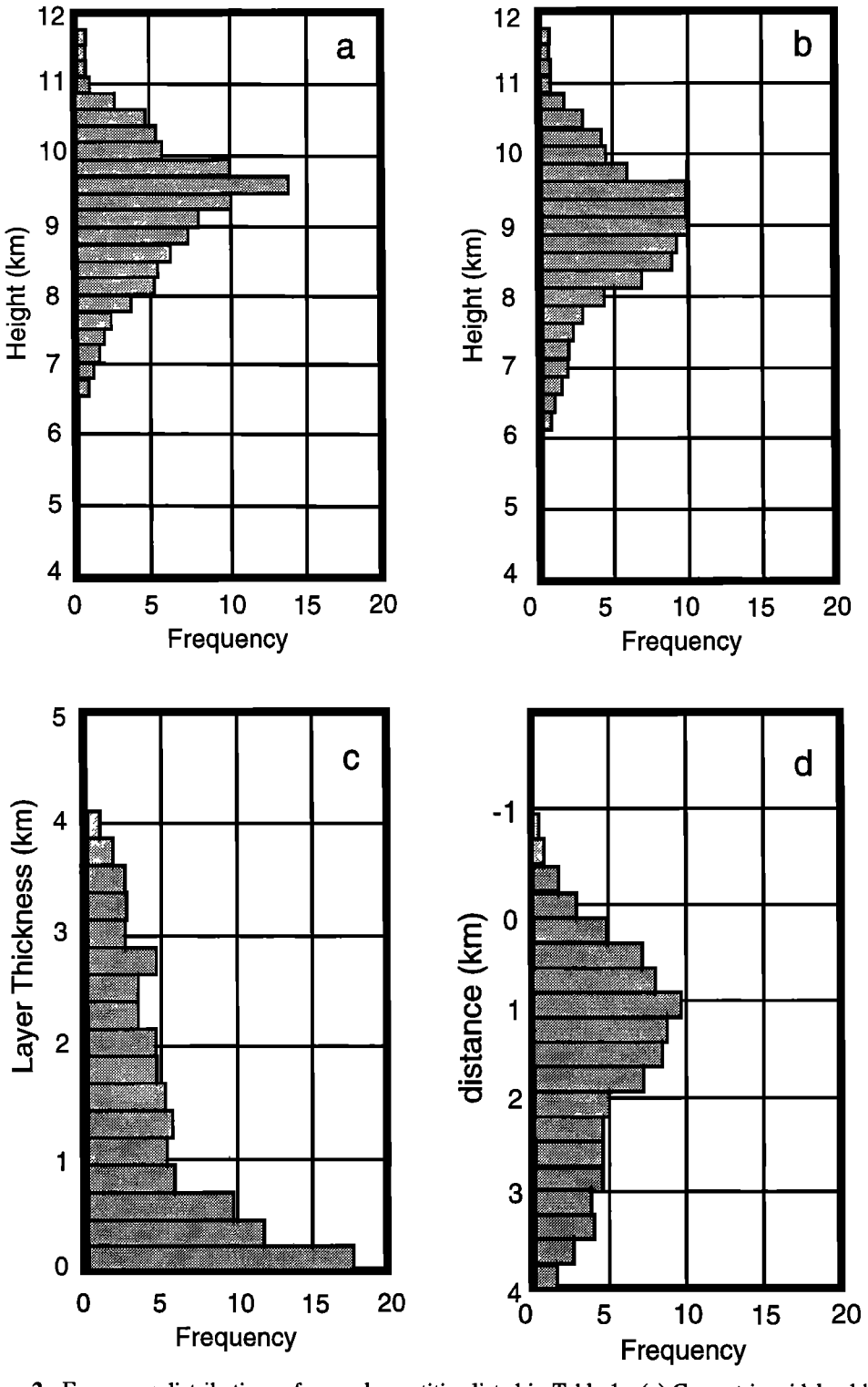

Figure 2. Frequency distributions of several quantities listed in Table 1. (a) Geometric midcloud height. (b) Reflectivity-weighted mid-cloud height. (c) Layer thickness. (d) Distance of cloud top from the tropopause. Positive distances are below the tropopause.

to identify cirrus layers (K. Sassen, personal communication, 1996]. However, since the radar was operated unattended for long periods and much of the cirrus observed by the radar occurred above overcast lower-level cloud decks, we are forced to define cirrus using the reflectivity data alone. We considered several height-dependent and temperature-dependent definitions; all of them produced similar results and lead to similar conclusions. The definition we use for this study is the least constrained by arbitrarily imposed boundaries and captures most of the cloud layers that would typically be defined as cirrus using visual inspection. For a cloud layer to be defined as cirrus we require only that the maximum reflectivity in that cloud layer occurs at a level with a temperature colder than -30°C. This definition of cirrus excludes cirrus-capped middle troposphere

clouds and precipitating cloud systems because the reflectivity profiles in such clouds maximize at warmer temperatures where large ice and precipitation particles are formed.

Results

Several fundamental statistics compiled from the radar time series are presented in Table 1 and Figure 2. During the approximately 2 months of data collection, nearly 1000 hours of radar data were acquired, and approximately 100 hours were removed from the dates by the selection criteria discussed above. In the remaining 900 hours, cirrus (as defined above) were observed during 288 hours or 32% of the time. This frequency of occurrence agrees well with the satellite study of *Wylie and Menzel* [1989], who found that cirrus fractional coverage over the continental United States ranges from 23 to 28%, although Wylie and Menzel did not segregate their data by cloud base temperature as was done here. Unlike *Wylie and Menzel* [1989], however, we did not detect any increase of cirrus clouds during daylight hours. Multiple cirrus cloud layers occurred during 61 of the 288 hours or 21% of the time, and cirrus occurred with lower-level cloud layers during 145 of the 288 hours or 51% of the time.

When considering these statistics, one must keep in mind that the reflectivity of some cirrus falls below the minimum detectable signal of the radar even with the long temporal averaging done here. *Atlas et al.* [1995] calculated theoretical radar reflectivities from observations of cirrus ice crystal distributions collected primarily by a King Air aircraft and found that 10% of the cirrus observed during the First International Satellite Cloud Climatology Project (ISCCP) Retional Experiment (FIRE) I had reflectivities below -35 dB Z_e. and 5% below -40 dB Z_e.. FIRE I took place during October and November of 1991 in Wisconsin, which is a similar climatological regime to that during this study. However, the King Air is generally limited to altitudes lower than about 9 km. The particle size distributions used in the Atlas et al. study may be biased toward warmer cirrus where the particle sizes would be larger and the reflectivities higher than for clouds above 9 km. The minimum detectable signal of the PSU radar at cirrus altitudes is illustrated in Figure 1 and ranges between -40 and -36 dB Z_e. We assume, therefore, that we miss no less than about 5% of the cirrus. However, this number is likely somewhat higher given the biases in the Atlas et al. study but is probably no more that 10-15% and is composed of the most tenuous cirrus containing the least ice mass. If we were to express this fraction of cirrus not detected by the radar in terms of the fraction of total ice water mass that occurs in the upper troposphere, we would find that the we are detecting well over 95% of this distribution. The possibility of undetected cirrus leads to unknown biases in the statistics shown in Table 1. For example, *Winker and Vaughn* [1994] performed extended lidar observations of cirrus at Hampton, Virginia, during the autumn of 1989 and spring of 1991. They report cirrus mean layer heights at 10-12 km and mean layer thicknesses between 0.86 and 0.94 km. The *Winker and Vaughn* [1994] results indicate cirrus to be slightly higher and thinner than the cirrus reported here, although their results may be biased due to attenuation of laser energy by thicker cirrus and low-level clouds. The results reported in Table 1 do tend to agree closely, however, with the compilation of *Dowling and Radke* [1990], who report an average cirrus cloud top altitude of 9-10 km, a cirrus mean layer thickness of 1.5 km, and typical cloud center altitudes of 9 km.

Frequency distributions of several of the quantities listed in Table 1 are illustrated in Figure 2. The geometric midcloud height tends to be constrained by the mean tropopause height and peaks near 9 km. The reflectivity-weighted midcloud height is similar except that the peak is shifted downward by about 0.5 km and is more broadly distributed. The difference between the geometric and reflectivity-weighted midcloud height distributions is due to the propensity for larger ice crystals of greater reflectivity to be nearer the base of cirrus layers. This issue will be discussed in greater detail below.

The tropopause appears to be an upper bound for the radar-observed cloud tops. Only a small fraction (approximately 1%) of the observed cirrus layers extend above the tropopause, and this probably represents our level of uncertainty in estimating the tropopause from the model output. The distribution peaks broadly at 1.25 km below the estimated tropopause height. Since the tops of some cirrus layers are below the minimum detectable signal of the radar, it is difficult to know if this statistic is accurate.

The frequency distribution of cirrus layer thickness is of particular interest. Nearly 50% of the observed cirrus layers have a thickness less than 1 km, while 25% of the cirrus layers have a thickness between 1 and 2 km and the remaining 25% are distributed between 2 and 6 km. This characteristic of cirrus cloud layers has direct implications for the parameterization of these clouds in atmospheric models. The vertical resolution in the upper troposphere of typical atmospheric models tends to be of the order of several kilometers. Cloud parameterizations in global circulation models must account for the subgrid characteristics of cirrus in the vertical if the radiatively important cloud top and base heights are to be properly represented in the models. This has been recognized by *Del Genio et al.* [1996], who found that a simple parameterization of this effect improves comparison of GCM results with ISCCP data. They also note that more work needs to be done on this problem.

Vertical Motion: Cirrus Occurrence Relationships

Slingo [1987] explored several conceptual approaches to the parameterization of non-convective clouds in large-scale models. These include static stability, relative humidity, and resolved-scale vertical motion. *Starr and Cox* [1980] investigated static stability as an indicator of cirrus occurrence using radiosonde data with vertical resolution similar to that of large-scale models. They concluded that static stability has poor correlative association with cirrus occurrence. Relative humidity is obviously an important predictor of cloud occurrence. However, we use model output to define the large-scale environment. Since we consider the model relative humidity prediction in the upper troposphere to be too sensitive to the model physical parameterizations and to uncertainties in radiosonde observations which the model assimilates, we do not consider it here. *Starr and Cox* [1985a] hypothesized that the large-scale vertical motion is an important element in the formation and maintenance of cirrus clouds and demonstrated this sensitivity using a cirrus model. *Heymsfield and Donner* [1990] synthesized the model of *Starr and Cox* [1985a] into a parameterization of cirrus clouds applicable to global circulation models. The Heymsfield-Donner parameterization, and others like it, is diagnostic and assumes that cirrus do not form in regions of large-scale subsidence. Using the mass divergence from the RUC model at a horizontal scale of 200 km and the kinematic technique, we find this assumption to be reasonably valid for most cirrus (Table 1), al-

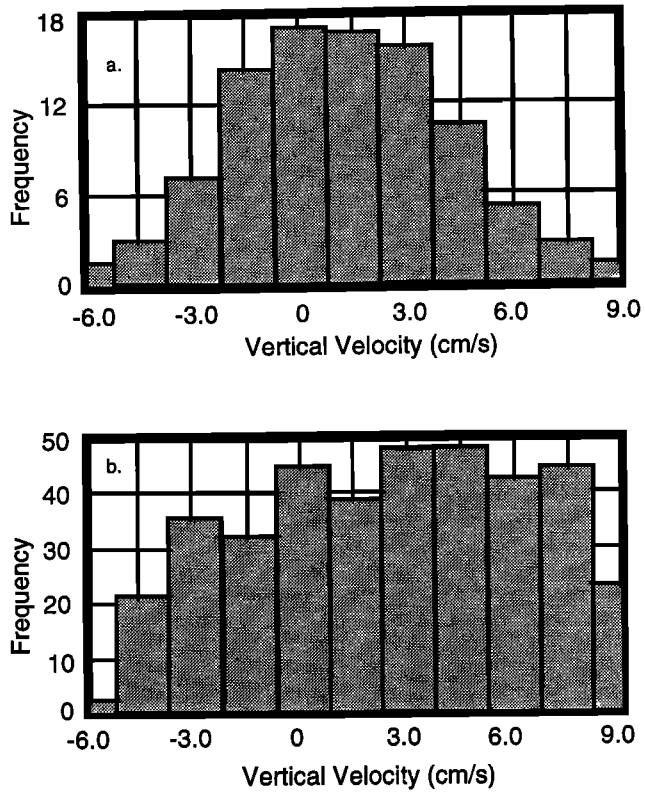

Figure 3. Relationship between observed cirrus and calculated synoptic scale vertical motion. (a) Distribution of vertical velocities calculated during cirrus observations. (b) Cirrus occurrence frequency as a function of vertical velocity. For example, when the vertical velocity was 4.5 cm/s, cirrus were observed 45% of the time.

though approximately 30% of the cirrus we observed occurred in regions of large-scale subsidence (Figure 3a). The distribution of large-scale vertical velocity associated with the cirrus observed during the autumn 1994 observation period tends to be broadly distributed about the mean listed in Table 1 with more than 60% of all cirrus layers occurring when the large-scale vertical motion is between 0 and +4.5 cm s^{-1}. The frequency of occurrence drops substantially for vertical motions greater than +4.5 cm s^{-1} and is a possible artifact of the data processing. In cases with large positive vertical motion, there is an increasing likelihood of the occurrence of thick lower-level clouds and precipitation, which leads to significant attenuation of the radar beam. As noted earlier, these cases were removed from the time series.

The frequency of cirrus occurrence as a function of large-scale vertical motion is shown in Figure 3b. The likelihood of encountering cirrus increases steadily as the large-scale ascent increases from -4.5 cm s^{-1}. A significant maximum of 45% occurs at +4.5 cm s^{-1}. We also examined histograms relating layer-mean reflectivity and large-scale ascent, but found no well defined relationship. This does not necessarily mean that a relationship between ice water content and vertical motion does not exist, but it certainly does not confirm this assumption. It is evident from these data that, while positive large-scale vertical motion appears to be important, positive large-scale ascent is neither a necessary nor sufficient condition for cirrus occurrence. A significant fraction of cirrus exists in regions of large-scale subsidence. We assume that these clouds are either advected over the radar from generation regions upstream of the radar or are formed in conditions where mesoscale or turbulent regions allow cirrus formation in areas where the larger-scale vertical motions are downward. *Starr and Wylie* [1990] diagnosed such a situation during the FIRE Cirrus I field campaign. Using radiosonde profiles to define the large-scale vertical motion, they found cirrus formation associated with mesoscale upward motions embedded within regions where the synoptic-scale vertical motions were unambiguously subsident.

Temperature-Reflectivity Relationships

More than 80% of the cirrus cloud observations occur between -35°C and -45°C and between -35 and -25 dB Z_e Plate 1). (Note that the radar's lack of sensitivity to reflectivities at cirrus levels below -35 dB Z_e leads to an under-representation of low reflectivity-low temperature cases.) Assuming that homogeneous nucleation is the primary formation mechanism at these temperatures [*Rogers and Yau*, 1989; *Sassen et al.*, 1985; *Sassen and Dodd*, 1988], supercooled water drops are nucleated in water-saturated updrafts, and spontaneous freezing occurs at temperatures colder than about -40°C. These newly formed ice crystals eventually begin to fall either because they are detrained from the updraft or their terminal velocity becomes sufficiently large with respect to the air motions due to depositional growth in the updraft. If the particles fall through air supersaturated with respect to ice, they continue to grow primarily by vapor deposition and secondarily by aggregation. Doppler velocity observations of cirrus particles collected during this study and others almost exclusively indicate downward particle motion, suggesting that it is during this settling phase of the particle life cycle that a cloud radar is sensitive enough to detect them. As an example, consider the fairly typical time series of cirrus reflectivities and Doppler velocities shown in Plate 2. A well developed fall streak is evident between 8 and 6.5 km from 1305 until 1313 UTC with maximum reflectivities reaching -15 dB Z_e. Weak upward Doppler motion is observed at and just above 8 km near 1309 UTC. At 1313 UTC, a deeper layer of ascending motion is indicated that extends from 7.5 to above 9 km. Following this, a period of higher reflectivities coupled with strong downward Doppler velocities persists from 1314 until 1319 UTC. This case bears strong resemblance to the cirrus uncinus generating cells investigated by *Heymsfield* [1975] and modeled by *Starr and Cox*, [1985a, 1985b]. The first event between 1305 and 1312 UTC appears to be a mature or decaying cell with only a weak area of ascending motion and an elongated fall streak, while the second event gives the impression of a developing generating cell. It is likely that the second region of higher reflectivities would continue to elongate vertically as the particles precipitate. In the identifiable updraft regions, where the radar reflectivities are weak, ice nucleation occurs as the particles are lofted to colder temperatures. After the particles are detrained from the updraft, growth continues as the particles settle through ice-supersaturated air. This is consistent with the higher reflectivities observed in the regions of downward Doppler motion.

Several empirically based parameterizations have been proposed that relate cirrus IWC and effective particle size to temperature [*Heymsfield and Donner*, 1990; *Heymsfield and Platt*, 1984] or to physical height in the atmosphere [*Slingo*, 1987]. In the distribution shown in Plate 1, we find only a very weak cor-

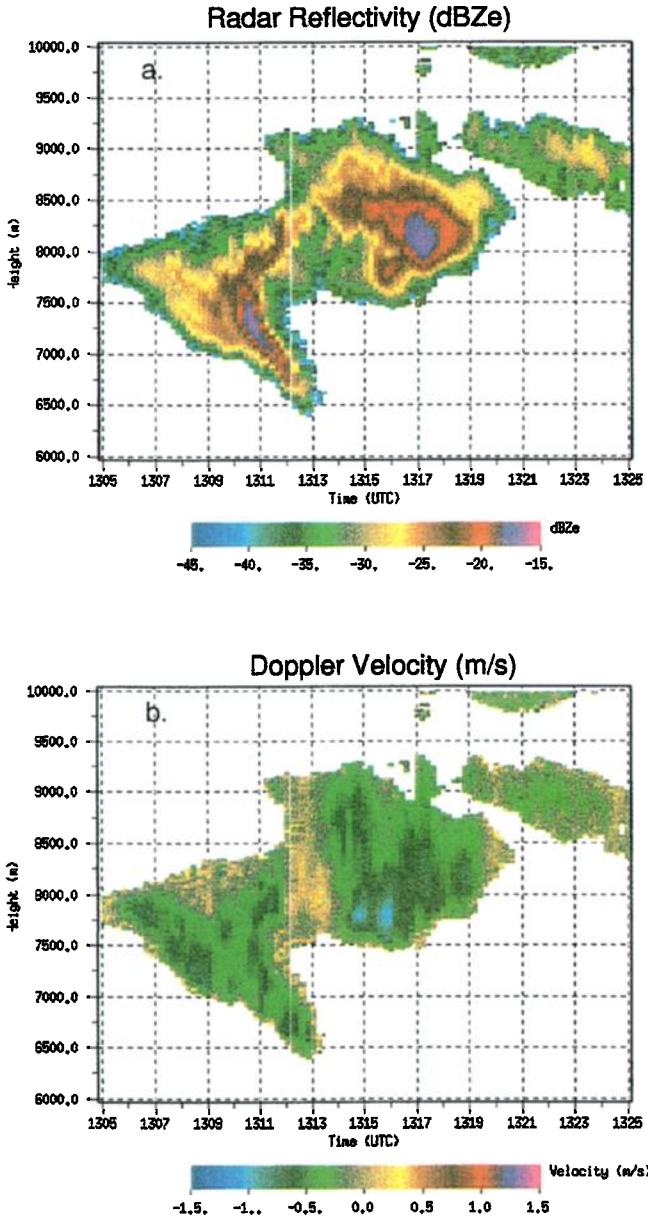

Plate 2. (a) Radar reflectivity and (b) Doppler velocity time-series that was observed on November 3, 1994.

relative relationship between reflectivity and temperature. Reflectivities do tend to be low at the coldest temperatures. However, at the warmer temperatures, the reflectivity frequency of occurrence is almost uniform from the lowest to the highest reflectivity values. *Atlas et al.* [1995] show that IWC and Z_e are proportional, but the constant of proportionality changes substantially between cirrus events. If the IWC-T parameterizations are valid, we would expect to find a more well-defined correlative relationship in Plate 1. These data strongly suggest that simple parameterizations of cirrus ice water content based on Clausius-Clapeyron relationships are erroneous. Similarly, predictive relationships between temperature and particle size appears to be highly questionable. *Heymsfield and Platt* [1984] propose a temperature-dependent size-distribution parameterization based on in situ aircraft data. They developed their parameterization, however, for spatial and temporal scales larger than those considered here. Assuming typical wind speeds at cirrus levels, the 50,000 pulse averages used in this study correspond to length scales of the order of 5-10 km. At these scales, temperature appears to be a poor predictor of particle size.

Similar conclusions can be reached by considering layer-mean quantities (Plate 3). We define a layer to be a set of vertically contiguous cloudy observations that meet the criterion described in the previous section. Although a positive correlation does exist between layer-mean temperature and layer-mean reflectivity, the correlation coefficient is negligible. Within the range of temperatures at which cirrus are observed to occur in these data, the temperature appears to have only a weak influence on the layer-mean radar reflectivity. On the basis of this observation we speculate that the layer-mean particle size is also essentially independent of temperature. When we segregate the layer-mean temperature versus layer-mean reflectivity histograms by layer thickness (Plate 4), it becomes evident that the mean reflectivity depends upon the depth of the layer, although there is a large amount of variation among events. A correlation between layer depth and layer-mean reflectivity should not be surprising given the above discussion. Cirrus crystals that grow as they settle through layers supersaturated with respect to ice reach larger sizes the longer they exist in such an environment. Because of the D^6 contribution to Z_e, these larger particles tend to dominate the layer-mean reflectivity.

Interestingly, a secondary mode to the layer-mean temperature versus layer-mean reflectivity distribution appears in Plate 3. This secondary component, marked by an arrow in Plate 3, occurs at warmer temperatures and somewhat lower reflectivities than the other observations and demonstrates a trend of decreasing reflectivity with increasing temperature. This region of the distribution accounts for about 10% of the total cirrus layers observed. As Plate 4 indicates, the majority of these layers are less than 1 km deep. We hypothesize that this secondary distribution is composed primarily of sublimating cirrus precipitation streamers settling through subsaturated air. The fallstreak between 1305 and 1312 UTC illustrated in Plate 2 falls into this classification. This particular layer is just over 1 km deep and occurred at a temperature between -28 and -33°C. The longevity of an ice crystal falling through subsaturated air depends on the local vertical air motions, the relative humidity of the air and the mass and density of the ice crystal [*Gultepe and Starr*, 1995]. *Hall and Pruppacher* [1976] calculate that a 160 μm ice crystal falling through environmental air with 50% relative humidity and zero mean vertical velocity can fall several kilometers before complete sublimation. *Starr and Wylie* [1990] and *Starr and Cox* [1985b] show that the sublimation of falling ice below the main cirrus generation layer leads to humidification and destabilization of the layer in which the sublimation occurs and often results in a downward migration of the main cloud generation layer and a progressive thickening of the cloud system. While these cirrus layers compose only a fraction of the total distribution, they are important components of the overall feedback of cirrus clouds because they redistribute water vapor within the troposphere and they can influence precipitation processes in midlevel water clouds.

Vertical Distribution of Reflectivity

The results in Plate 4 suggest that the layer-mean reflectivity of a cirrus layer is somewhat dependent on the geometrical depth of the layer and a likely indicator of the particle sizes that evolve within a layer of given thickness. However, the vertical distri-

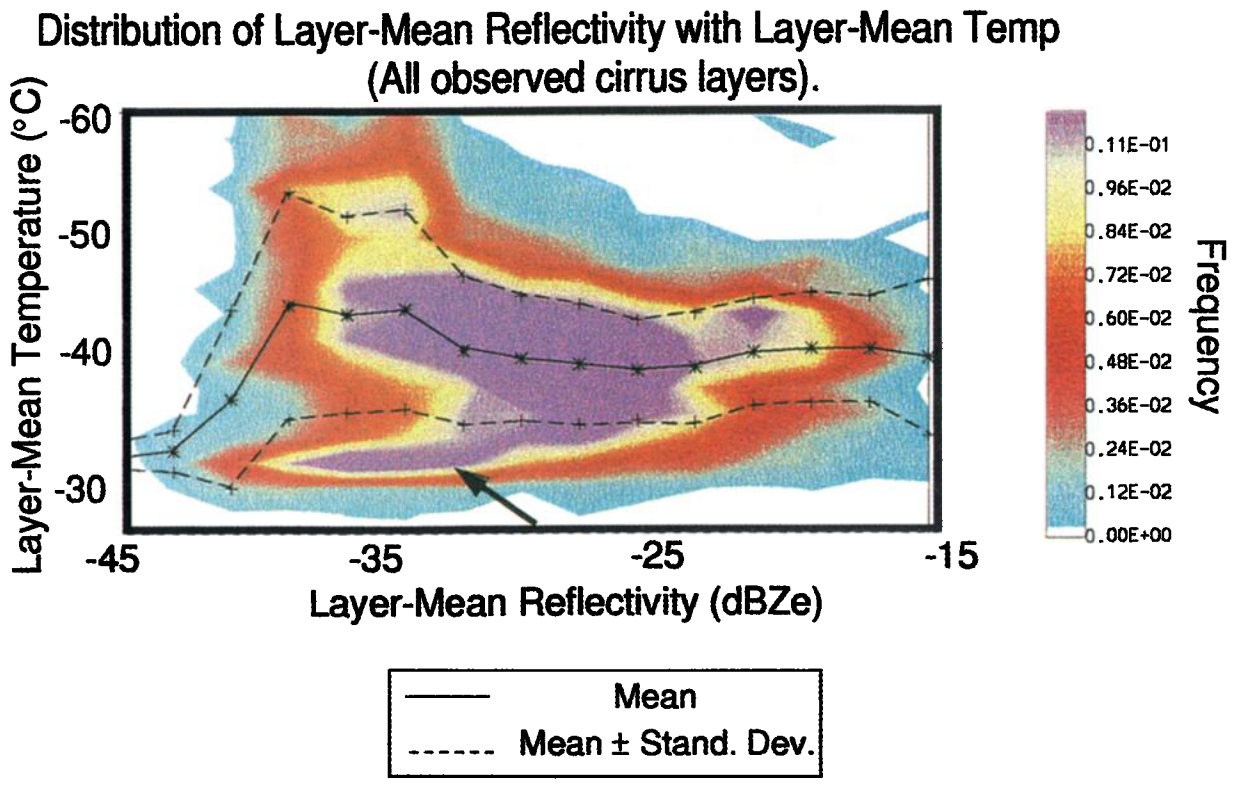

Plate 3. Frequency histogram of cirrus layer mean temperature and layer-mean reflectivity for all cirrus layers observed during the autumn 1994 observing period. The arrow denotes a secondary distribution discussed in the text. The solid and dashed lines are as in Plate 1.

bution of ice water and particle size within a layer is an important factor in determining the cirrus layer's radiative characteristics. For instance, *Vogelmann and Ackerman* [1995] show that the mass extinction cross section and single scattering albedo at thermal infrared wavelengths are sensitive to effective particle size. Since cirrus are known to have a strong influence on the longwave cooling to space due to their location in the upper troposphere, the vertical distribution of ice mass and particle size within a layer determines the effective radiative temperature of the layer and thus the ultimate climatic influence of the cloud.

To examine the vertical distribution of radar reflectivity within the observed cirrus layers, we determine the vertically integrated reflectivity of a given layer. Dividing each layer into 10 sublayers of equal geometrical thickness, we calculate the fraction of the vertically integrated reflectivity within each sublayer. A two-dimensional histogram corresponding to the sublayer location within the cloud and the fraction of the vertically integrated reflectivity within each sublayer is created by applying this algorithm to all cirrus layers (Plate 5). Note that the actual geometric width of any individual decile depends on the actual thickness of the cloud layer being considered. Although the variance of the reflectivity within each sublayer is large, some generalizations can be made. First, reflectivity tends to be unevenly distributed within cirrus layers. On average, the fraction of the integrated reflectivity within the top decile of the cloud layer tends to be a minimum. The decile reflectivity then increases to the decile at or just below the midpoint of the layer and then decreases again to the base of the cloud layer. The amplitude of this trend in the vertical distribution of reflectivity tends to be a strong function of layer thickness. For layers between 3 and 6 km thickness (approximately 10% of the total), the upper portions of the layer generally contain very little of the total reflectivity. This characteristic of thick cirrus layers is true in nearly all cases as can be seen by noting the high frequency of occurrence of low fractions of layer-integrated reflectivity in the histograms near cloud top. The fraction of the total reflectivity contained in the middle third of clouds thicker than 1 km is highly variable and averages approximately 40% of the total. By comparison, the reflectivity is somewhat more evenly distributed within cirrus of less than 1 km thickness (roughly half of all layers observed) and the variance of this distribution is nearly constant within the layer.

The vertical distribution of reflectivity shown in Plate 5 is directly related to the distribution of the relative particle sizes within cirrus and results from the growth and sublimation of ice crystals within the layer. Relatively small ice crystals near cloud top grow by vapor deposition and aggregation as they settle through ice supersaturated layers; their eventual size is determined by the time spent in the saturated air. Sublimation ensues as these ice crystals settle into subsaturated air. The humidity of the subsaturated air and the particle size determines the crystal longevity. The cirrus cloud layer shown in Plate 2 illustrates this interpretation and also shows the degree of variability that exists even within particular cases. The deeper portions of the uncinus cells at 1310 and 1317 UTC tend to have reflectivity profiles weighted by the -15 dB Z_e maxima near 7250 and 8000 m, respectively. These maxima occur near the middle portions of the layer. The impression of sublimation is particularly strong in the first fall streak (after 1311 UTC) where the reflectivity decreases steadily as the fallstreak descends into a vertical wind

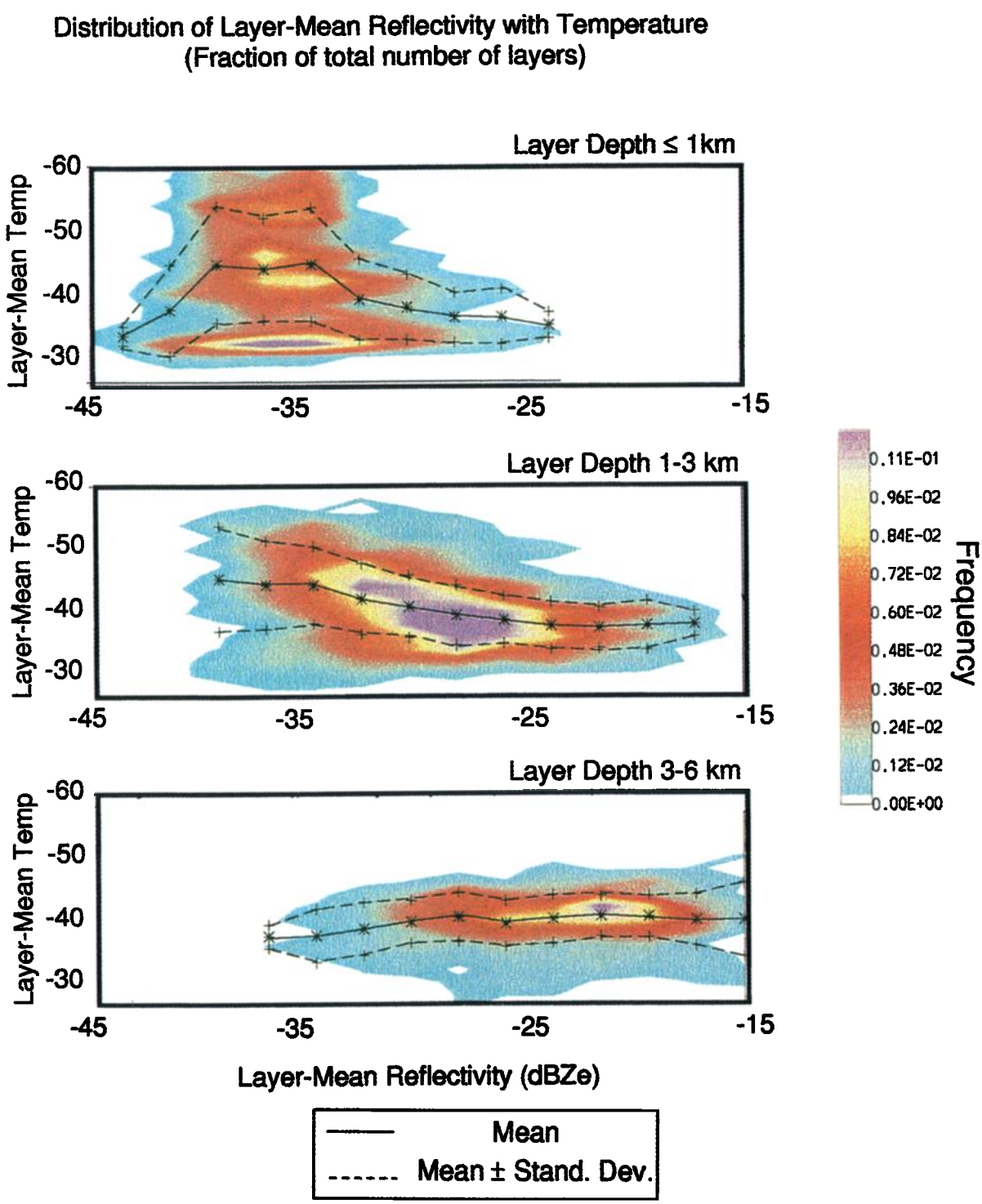

Plate 4. As in Plate 3, except segregated by layer depth.

shear. The thinner portions of the cirrus layer (between 1305 and 1307 and after 1319 UTC) show a much more even vertical distribution of reflectivity.

The interpretation of Plate 5 is supported by other observational and modeling studies of cirrus microphysics. *Miloshevich et al.* [1993], for instance, used balloon-borne crystal replicators to examine the microphysical structure of cirrus during FIRE II. Their data show crystal growth between cloud top and midcloud while also showing evidence for sublimation near cloud base. Doppler velocity observations of cirrus crystals typically show a decrease in reflectivity and an increase in fall velocity near cloud base. As crystals sublimate, the sharp edges of the hexagonal cirrus crystals become more rounded [*Miloshevich et al.*, 1993] and their aerodynamic characteristics change. The sublimating particles fall more like spheroids, that is, faster, and their reflectivity decreases due to decreasing particle size. This is evident in Plate 2 where the maximum downward Doppler motions occur near the base of the layer at 1308 and 1315 UTC and do

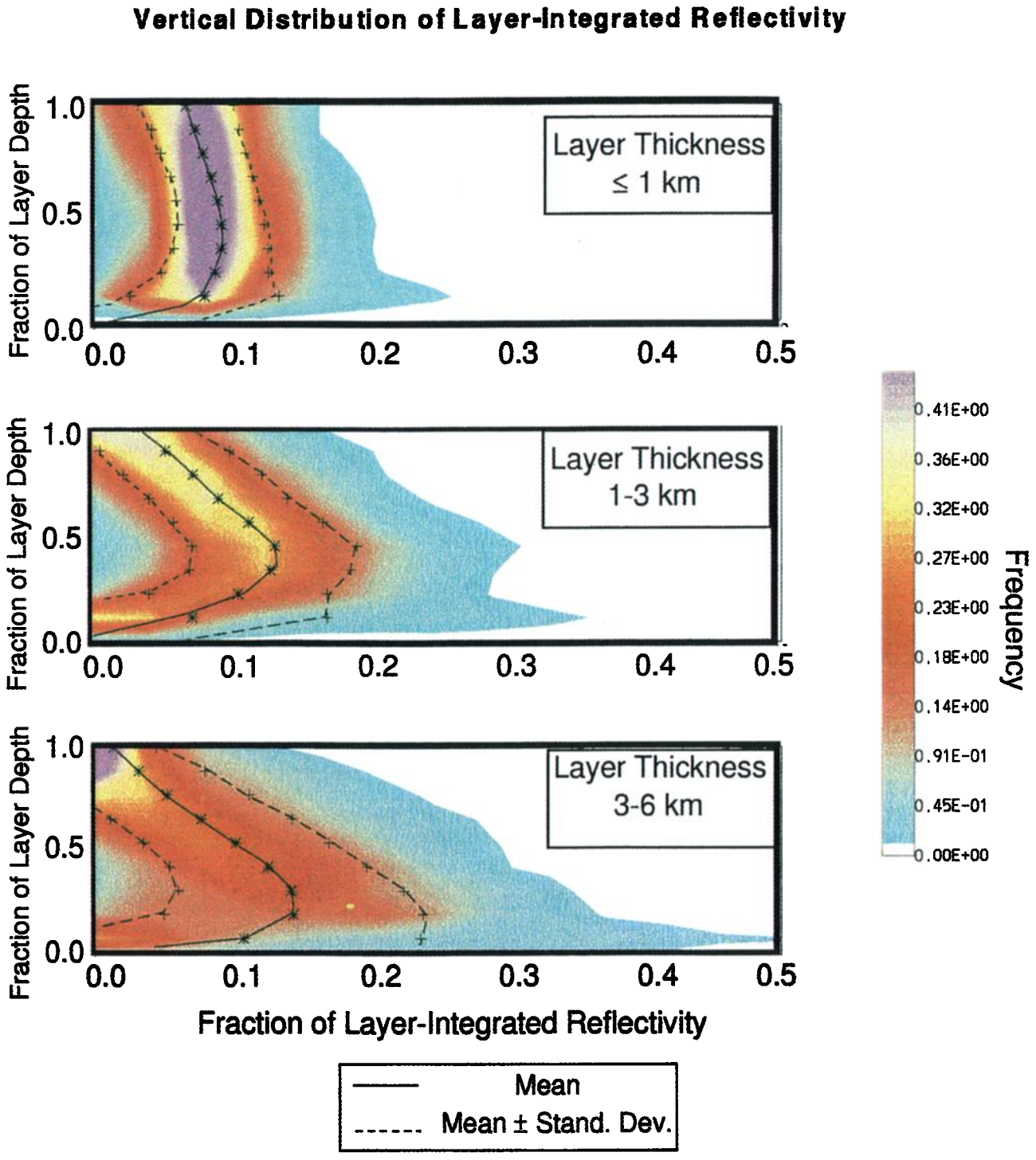

Plate 5. Frequency histograms depicting the vertical distribution of radar reflectivity within cirrus layers of indicated thickness. See text for explanation. The solid line indicates the mean fraction of the layer-integrated reflectivity in that decile of the layer. The dashed lines denote plus and minus 1 standard deviation from the mean.

not occur in conjunction with maxima in reflectivity. The distribution shown in Plate 5 suggest that, regardless of layer thickness, sublimation tends to occur in the bottom third of the layer. The larger cirrus crystals precipitating into the sublimation zone in a deep cloud survive considerably longer than do the smaller crystals settling into the sublimation zone of thin cirrus layers [*Hall and Pruppacher*, 1976; *Gultepe and Starr*, 1995].

This interpretation of the vertical distribution of radar reflectivity helps explain the weak correlation identified between temperature and reflectivity in Plates 1 and 3 and also explains the strong dependence of layer-mean reflectivity on layer depth seen in Plate 4. Assuming that homogeneous nucleation of cirrus is the primary formation mechanism, cirrus crystals are nucleated at temperatures colder than approximately -40°C in up-

drafts supersaturated with respect to liquid water. These crystals grow by vapor deposition and are eventually detrained from the updraft or settle due to increasing mass. The evolution of the cloud layer is then determined primarily by the ice supersaturation of the layers through which the cirrus crystals precipitate. In simple terms, the crystals grow as long as they reside in air supersaturated with respect to ice with the growth rate determine by particle size, number concentration, and humidity as well as the subsequent dynamical forcing induced by radiation and latent heat exchange within the cloud layer. Temperature is important only to the extent that the supersaturation depends on it, and simple parameterizations of cirrus characteristics based solely on temperature will fail to capture the mechanisms that dictate the evolution of the cloud layer. Model parameterizations must take into account the water vapor and turbulent structure of the upper troposphere in order to adequately predict cirrus properties.

Application to Satellite Radar

The obvious utility of ground-based radar has led to serious consideration of plans for a satellite-borne 94-GHz radar (CLOUDSAT Science Team Planning Workshop, Jet Propulsion Laboratory, September 1996]. Current engineering studies indicate that a radar on a polar-orbiting satellite could be built with 500 meter vertical resolution and a minimum detectable signal of -36 dB Z_e in the upper troposphere. The horizontal footprint of such a system would be of the order of 1 km by 2 to 4 km. The obvious questions that follow are what fraction of existing cirrus would be seen by a radar with these characteristics and how would the statistics of the resulting cirrus climatology differ from what is reported above.

To address these issues, we degrade the vertical and temporal resolution of the autumn 1994 data to match the characteristics of a satellite radar system. Matching the horizontal footprint of a space-based radar with a surface based vertical time series is problematic. Using the wind speed in the upper troposphere predicted by the RUC model, the radar data were temporally averaged to match a 3-km along-stream distance. While this does not exactly reproduce a spatial sample, it more faithfully captures the horizontal averaging that will be inherent in a satellite system. The vertical resolution of the temporally averaged profiles were then degraded to match the 500-m vertical resolution of a satellite system. In the temporal and vertical averaging process, only the cloudy Z_e values contributed to the summed Z_e. This summed Z_e was then divided by the total number of observations, clear and cloudy, in the interval under consideration to obtain the degraded value of Z_e. Only those resulting observations with a reflectivity greater than -36 dB Z_e were retained.

The statistics of the simulated satellite database are shown in Table 2. Comparing Tables 1 and 2 shows that the satellite radar would see about two thirds of the cirrus layers detected with the ground-based system. A considerable part of this decrease is simply attributable to the relatively coarse vertical resolution of the satellite system. Since our observed dB Z_e values are almost all below -20 dB Z_e and many of the layers are thinner than 0.5 km, the satellite tends not to detect cirrus in partially filled volumes. In addition to missing the thinner layers, the satellite radar would also fail to detect the tops and bottoms of thicker, more reflective layers. This is evident by the slightly lower cloud top, slightly higher cloud base, and identical midcloud height. Interestingly, the mean thickness of the simulated satellite data is smaller than that observed by the ground-based system. This mean thickness corresponds to just less than 3 range gates for the satellite system. This is an artifact, however, of the degraded sampling. Since the maximum vertical resolution of the satellite radar is 500 m, any thin but highly reflective layers in the ground-based data would be assigned a 500-m thickness. Also, the thickness of many layers observed by the ground-based system are reduced substantially in the satellite data since the tops and bottoms of these layers are below the detectability threshold of the satellite system.

Table 2. Cirrus Occurrence Frequencies, Means, and Standard Deviations Using Space-Borne Radar Specifications

	Mean	Standard Deviation
Fraction of observations, %	21	
Cirrus base, km	8.6	1.0
Cirrus top, km	9.7	1.1
Midcloud height, km	9.2	0.8
Layer thickness, km	1.5	1.1
Temperature, °C	-40	9.0
Reflectivity, dB Z_e	-24.5	-23.0

As in Table 1, except that the original data set was degraded in resolution assuming the specifications of a proposed satellite-borne 94-GHz radar.

The logical conclusion to be drawn from this simulation is that a lidar should be flown along with a satellite radar. A small lidar system would be quite capable of detecting the thin cirrus that falls below the radar threshold and would identify the correct cloud top height [*Sassen*, 1991]. However, the lidar would be unlikely to penetrate the thicker cirrus cases and would fail to detect the substantial fraction of low cloud events found in conjunction with thick cirrus. Also, because this data were acquired in the late autumn, they contain no cirrus directly generated by deep convection. Our experience with convective cirrus, particularly in the tropics, indicates that it often occurs in deep, optically thick layers. These layers would be more deeply penetrated by the radar, but not by the lidar.

Conclusions

We have examined cirrus cloud characteristics observed by a 94-GHz radar during an extended observational period from early October through late December 1994 and interpret the observed reflectivities in the context of a continuous representation of large-scale meteorology gleaned from the RUC model output. The fundamental statistics of the cirrus observed during this period are listed in Table 1 and agree quite well with similar statistics compiled by *Dowling and Radke* [1990], *Wylie and Menzel* [1989], *Uttal et al.* [1995], and *Winker and Vaughn* [1994]. The principal findings of this study are as follows:

1. On average, the cirrus observed during this period existed in environments in which the large-scale atmosphere was weakly ascending (Figure 3). However, approximately 40% of the cirrus occurred in situations where large-scale subsidence was occurring. Cirrus parameterizations based on model-resolved vertical motions must account for the possibility that cirrus may form and advect through environments that are subsiding at horizontal scales comparable to the model resolution.

2. Cirrus tend to occur in thin layers (Figure 2d). Approximately half of all layers observed during the observational period were less than 1 km deep. Considering the possibility that some fraction of thin cirrus is below the minimum detectable signal of the radar, the frequency distribution shown in Figure 2d may be biased on the low side for the thinner layers. To properly account for the radiative characteristics of cirrus clouds (particularly in the infrared), it is critically important that the cloud base and top be properly represented [*Vogelmann and Ackerman*, 1995].

3. We find little correlation between temperature and radar reflectivity (Plates 1 and 3). The mean reflectivity of cirrus layers does, however, seem to be a strong function of layer depth (Plate 4) with thicker layers attaining significantly higher reflectivity. Regardless of layer thickness, reflectivity tends to increase between cloud top and the middle regions of the cloud and then decrease in the lower third of the layer (Plate 5) with this trend being amplified in the thicker layers. On the basis of this vertical distribution, we infer that crystal growth tends to occur in the upper two thirds of most cirrus layers while the lower third is dominated by ice crystal sublimation. We further conclude that the principal elements important to the macroscale properties of cirrus cloud layers are the water vapor and turbulence structure of the regions at and below the nucleation zone. Parameterizations of cirrus properties based primarily on temperature do not account for this structure and likely lead to significant error in predicted radiative heating rates and in the redistribution of water vapor within the model atmosphere.

4. A radar with the sensitivity of a proposed satellite-borne W-band system would have detected approximately two thirds of the cirrus observed by our ground-based radar (Tables 1 and 2). We are uncertain what fraction of thin cirrus that occurred during this observational period was below the detectability limits of our radar. A satellite-borne W-band radar would tend to miss the more tenuous bases and tops of thicker cirrus layers while thinner layers might be completely undetected. In order to arrive at robust descriptions of cirrus distributions, a satellite-borne radar system should be accompanied by a lidar.

The results presented here are an analysis of only a 2-month cloud radar data set. In addition to the specific points above, two general conclusions can be drawn from this work. The first is that cloud radar is a unique tool for carrying out such studies. The radar was operated basically continuously whenever clouds were present. Thus the cirrus statistics are temporally complete. They are not subject to interruptions caused by the need for an operator or biased by obstruction due to low clouds. These features of a radar cirrus climatology lead to a significant advantage over all other climatologies. The Atmospheric Radiation Measurement (ARM) program, sponsored by the Department of Energy, has installed a continuously operating, vertically pointing 35-GHz radar at its site in north central Oklahoma. This radar, and those planned for other ARM sites, will produce the data needed to generate long-term statistics similar to those presented here.

The second general point is that the cirrus statistics show a large degree of variance in every statistical property that we examined. The large variations in properties, such as the reflectivity, suggest that there are correspondingly large variations in the radiative impact of the cirrus on both solar and infrared radiation fluxes at the Earth's surface and the top of the atmosphere as well as the radiative heating rates within the cloud layer. Parameterizations of cirrus in climate models must predict the variations in microphysical and radiative properties if they are to produce realistic simulations. At this point, we do not completely understand the linkages between the cirrus properties and the environmental conditions that produce them. The relationships investigated here suggest that many of the simple conceptual relationships used in current parameterizations are not completely correct. Some tantalizing indications of relationships can be inferred from these data, as we suggest in item 4 above. Unfortunately, the data set is too limited to allow us to extract their exact nature. We expect that additional data collection, including rigorous definition of large-scale environmental fields, will allow us to quantify these relationships and develop more robust parameterizations.

Acknowledgments. Dennis Lamb and Johannes Verlinde provided valuable criticism of this work from its inception, and we are grateful for their continued interest. We also wish to acknowledge the many useful suggestions provided by David Starr and Taneil Uttal. The data used in this study could not have been collected without the able assistance of our technical staff at the University, most particularly Robert Peters, who is largely responsible for the construction of the 94-GHz radar used in this study. This research was supported by the Environmental Science Division of the U.S. Department of Energy (grant DE-FG02-90ER61071), National Science Foundation Grant ATM-9317371, and NASA grants NAG-1-999 and NAG-5-2701.

References

Atlas, D., S.Y. Matrosov, A.J. Heymsfield, M.-D. Chou, and D.B. Wolff, Radar and radiation properties of ice clouds, *J. Appl. Meteorol.*, *34*, 2329-2345, 1995.

Benjamin, S. G., K. A. Brewster, R. Brummer, B. F. Jewett, T. W. Schlatter, T. L. Smith, and P. A. Stamus, An isentropic three-hourly data assimilation system using ACARS aircraft observations, *Mon. Weather Rev.*, *119*, 888-906, 1990.

Clothiaux, E. E. et al., An evaluation of a 94-GHz radar for remote sensing of cloud properties, *J. Atmos. Oceanic Technol.*, *12*, 201-229, 1995.

Del Genio, A. D., M. Yao, W. Kovari and K. K.-W. Lo, A prognostic cloud water parameterization for global climate models, *J. Clim.*, *9*, 270-304, 1996.

Doviak, R. J. and D. S. Zrnic, *Doppler Radar and Weather Observations*, 562 pp., Academic Press, San Diego, Calif., 1993.

Dowling, D. R. and L. F. Radke, A summary of the physical properties of cirrus clouds, *J. Appl. Meteorol.*, *29*, 970-978, 1990.

Gultepe, I. and D. O'C. Starr, A comparison of evaporative cooling with infrared heating beneath a cirrus cloud, *Atmos. Res.*, *35*, 231-271, 1995.

Hall, W. D. and H. R. Pruppacher, The survival of ice particles falling from cirrus clouds in subsaturated air, *J. Atmos. Sci.*, *33*, 1995-2006, 1976.

Heymsfield, A. J., Cirrus uncinus generating cells and the evolution of cirriform clouds, I; Aircraft observations of the growth of the ice phase, *J. Atmos. Sci.*, *32*, 799-808, 1975.

Heymsfield, A. J. and L. J. Donner, A scheme for parameterizing ice-cloud water content in general circulation models, *J. Atmos. Sci.*, *47*, 1865-1877, 1990.

Heymsfield, A. J. and C. M. R. Platt, A parameterization of the particle size spectrum of ice clouds in terms of ambient temperature and the ice water content, *J. Atmos. Sci.*, *41*, 846-855, 1984.

Hoskins, B. J., M. E. McIntyre, A. W. Robertson, On the use and significance of isentropic potential vorticity maps, *Q. J. R. Meteorol. Soc.*, *111*, 877-946, 1985.

Kropfli, R. A. et al., Cloud physics studies with 8mm wavelength radar, *Atmos. Res..*, *35*, 299-313, 1995.

Mace, G.G., D. O'C. Starr, T. P. Ackerman, and P. Minnis, Examination of coupling between an upper-troposphere cloud system and synoptic-scale dynamics diagnosed from wind profiler and radiosonde data, *J. Atmos. Sci.*, *52*, 4094-4127, 1995.

Miloshevich, L. M., A. J. Heymsfield and P. M. Norris, Microphysical measurements in cirrus clouds from ice crystal replicator sondes launched during FIRE II, Paper presented at 11th International Conference on Clouds and Precipitation, Amer. Meteorol. Soc., Montreal, Que., Canada, 1993.

Ramanathan, V., R. D. Cess, E. F. Harrison, P. Minnis, B. R. Barkstrom, E. Ahmad, and D. Hartman, Cloud-radiative forcing and climate: Results from the Earth radiation budget experiment. *Science, 243*, 57-63, 1989.

Randall, D., B. A. Albrecht, S. Cox, D. Johnson, P. Minnis, W. Rossow, and D. O'C. Starr, On FIRE at ten, *Rev. Geophys.*, in press, 1995.

Rogers, R. R. and M. K. Yau, *A Short Course in Cloud Physics*, 293 pp., Pergamon , Tarrytown, N. Y., 1989.

Sassen, K., K. N. Liou, S. Kinne and M. Griffin: Highly supercooled cirrus cloud water, Confirmation and climatic implications. *Science, 227*, 411-413, 1985.

Sassen, K., The polarization lidar technique for cloud research: A review and current assessment, *Bull. Am. Meteorol. Soc., 72*, 1848-1866, 1991.

Sassen, K. and G. C. Dodd, Homogeneous nucleation rate for highly supercooled cirrus cloud droplets, *J. Atmos. Sci., 45*, 1357-1369, 1988.

Sekelsky, S. M. and R. E. McIntosh, Cloud observations with a polarimetric 33 GHz and 95 GHz radar, *Meteorol. Atmos. Phys., 58*, 123-140, 1996.

Schroeder, J. A., and E. R. Westwater: Users' guide to WPL microwave radiative transfer software, *NOAA Tech. Memo. ERL WPL-213*, 84 pp., Environ. Technol. Lab., Boulder, Colo., 1991.

Slingo, J. M., The development and verification of a cloud prediction scheme for the ECMWF model, *Q. J. R. Meteorol. Soc., 113*, 899-927, 1987.

Starr, D. O'C. and S. K. Cox: Characteristics of middle and upper troposphere clouds as deduced from rawinsonde data, *Atmos. Sci. Pap.* 327, 71 pp., Colo. State Univ., Fort Collins, 1980.

Starr, D. O'C. and S. K. Cox: Cirrus clouds. I; A cirrus cloud model, *J. Atmos. Sci., 42*, 2663-2681, 1985a.

Starr, D. O'C. and S. K. Cox, Cirrus clouds. II; Numerical experiments on the formation and maintenance of cirrus, *J. Atmos. Sci., 42*, 2663-2681, 1985b.

Starr, D. O'C and D. P. Wylie, The 27-28 October 1986 FIRE cirrus case study: Meteorology and clouds, *Mon. Weather Rev., 118*, 2259-2287, 1990.

Stephens, G. L., S. Tsay, P. W. Stackhouse, Jr., and P. J. Flatau, The relevance of the microphysical and radiative properties of cirrus clouds to climate and climatic feedback, *J. Atmos. Sci., 47*, 1742-1753, 1990.

Thiebaux, H. J. and M. A. Pedder, *Spatial Objective Analysis, With Applications in Atmospheric Science*, 299 pp., Academic, San Diago, Calif., 1987.

Uttal, T., E. E. Clothiaux, T. P. Ackerman, J. M. Intrieri, and W. L. Eberhard, Cloud boundary statistics during FIRE II, *J. Atmos Sci, 52*, 4276-4284, 1995.

Vogelmann, A. M. and T. P. Ackerman, Relating cirrus cloud properties to observed fluxes: a critical assessment, *J. Atmos. Sci., 52*, 4285-4301, 1995.

Winker, D. M. and M. A. Vaughn, Vertical distribution of clouds over Hampton, Virginia observed by lidar under the ECLIPS and FIRE ETO programs, *Atmos. Res., 34*, 117-133, 1994.

Wylie, D. P. and W. P. Menzel, Two years of cloud cover statistics using VAS, *J. Clim., 2*, 380-392, 1989.

T. P. Ackerman and E. E. Clothiaux, Department of Meteorology and Earth System Science Center, The Pennsylvania State University, University Park, PA 16802. (email: ackerman@essc.psu.edu; cloth@essc.psu.edu)

B. A. Albrecht, Rosenstiel School of Marine and Atmospheric Science, University of Miami, 4600 Rickenbacker Causeway, Miami, FL 33149-1098. (email: balbrecht@rsmas.miami.edu)

G. G. Mace, Department of Meteorology, University of Utah, 819 Wm. C. Browning Bldg., Salt Lake City, UT 84112. (email: mace@atmos.met.utah.edu)

(Received June 5, 1996; revised November 20, 1996; accepted December 11, 1996.)